Role of Coulomb interactions on the electronic properties of monolayer NiX_2 (X = S, Se): A DFT+U+V study

Sergio Bravo,* P. A. Orellana, and L. Rosales
Departamento de Física, Universidad Técnica Federico Santa María, Av. Espana 1680, Casilla Postal 110V, Valparaíso, Chile

(Received 4 August 2023; revised 2 October 2023; accepted 30 November 2023; published 12 December 2023)

The electronic structure of nickel dichalcogenides, NiS_2 and $NiSe_2$, in monolayer form, is studied employing first-principles methods. We assess the importance of band ordering, covalency, and Coulomb interactions in the ground state of these systems. Hybrid functional results are compared with standard functionals and also with Hubbard-corrected functionals to systematically address the role of electronic interactions and localization. Using empirical as well as linear response derived and modified parameters, we found that mean-field correlations realized by intersite Hubbard interactions are directly linked to the magnitude of the energy band gap. This gives compelling evidence that the DFT+U+V method is suitable to describe the charge transfer insulating phase in these materials.

DOI: 10.1103/PhysRevB.108.235138

I. INTRODUCTION

Two-dimensional (2D) van der Waals materials have emerged as a class of systems that have proven to hold great potential for realizing new physics as well as novel technological capabilities. Among the families that have aroused a high level of interest in recent times, the transition metal dichalcogenides (TMDs) stand out. They exhibit an attractive combination of atomic-scale thickness, strong spin-orbit coupling, direct band gap, and favorable electronic and mechanical properties [1]. This makes them interesting for basic research and, for example, high-end electronics and spintronics applications.

Even with these advances, there remain many 2D TMDs that deserve to be investigated in more detail. To this category belong the nickel dichalcogenides NiX_2, with X = S, Se, Te. This group of materials has been proposed theoretically [2,3] in the 2H and 1T phases and also realized experimentally, in the case of 1T $NiSe_2$ [4]. The properties studied are related to band engineering [5], thermoelectric efficiency [6], and anode materials in batteries, and also superconductivity [7].

One of the ingredients that is lacking in these recent studies is the inclusion of electronic interactions. As we know, the presence of localized d orbitals in transition metals makes it necessary that the correlation effects are accounted for so the predicted physical properties are closer to reality. The level of refinement in the treatment of interactions varies widely, and factors that impact the selection of a method stems from the size of the system, the type of the components, and the available computational resources. Examples of methods that treat the interacting problem are the Hartree-Fock approximation [8], GW approximation [9], mean-field approximations [10], density functional theory (DFT) [11], dynamical mean-field theory [9] and coupled cluster theory [12], which form just a limited list. Among the possible methods mentioned, mean-field methods along with DFT, are the fastest and most flexible in computational terms. This allows us to study systems with considerable sizes and different kinds of structures without high cost. Inside the DFT framework, one of the implementations of electronic interactions at the mean-field level that is widely used is known as Hubbard-corrected DFT or DFT+U, for its early implementation [13,14]. This formalism adds a minimal term to the original DFT energy functional, which accounts for on-site Coulomb repulsion (U) at the atoms with localized orbitals [14]. This approach has been very successful and, in recent years, it has been implemented in extended form by including not only on-site parameters but also intersite interactions [15–17]. This last method is starting to be used in studies of different materials [18–23], giving unique perspectives on the incidence of interactions on the electronic structure.

To study the effects of correlation in the NiX_2 systems, in this paper, we employ DFT with Hubbard corrections and also with hybrid functionals to characterize NiS_2 and $NiSe_2$ in the 1T monolayer form. We carry out a band-structure study in momentum space along with real-space orbital characterization to explore the role of Coulomb interaction in these systems at the mean-field level. A complementary charge transfer phase is identified in both materials and its origin is discussed.

The paper is organized as follows. First, we detail the computational resources and corresponding settings for the first-principles calculations. Next, we mention the more salient structural properties of NiX_2 in Sec. III A. The calculations using the noncorrected DFT methods are presented in the Sec. III B along with the results of the electronic structure using a hybrid functional. Also, we present a discussion of the basic electronic features. This is followed in Sec. III C by describing the main method used in the work, namely, the application of the Hubbard-corrected DFT method. Next, in Sec. III D, we outline the results for the magnetic phase

*sergio.bravoc@usm.cl

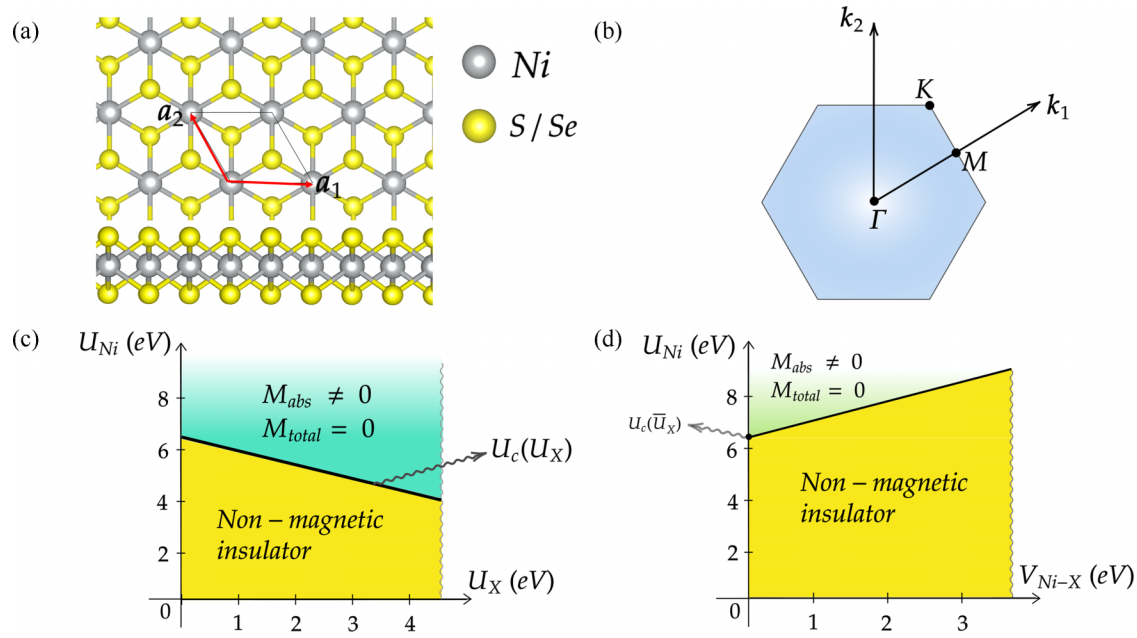

FIG. 1. (a) The lattice structure of monolayer NiX_2. (b) Two-dimensional Brillouin zone for the monolayer NiX_2 systems. (c) Magnetic phase diagram for U_{Ni} versus U_S for fixed intersite interactions V_{ij}. The range of values for U_{Ni} was taken from 0 eV to 9 eV and U_X was taken from 0 to 4 eV. $U_C(U_X)$ defines a line where the magnetic phase transition occurs. (d) Magnetic phase diagram for U_{Ni} versus $V_{\mathrm{Ni}X}$ for fixed on-site interaction $\bar{U}_X$. The range of values for U_{Ni} was taken from 0 eV to 9 eV and $V_{\mathrm{Ni}X}$ was from 0 to 3 eV.

diagrams for the materials and motivate the approach to construct suitable sets of parameters. In Sec. III E, the self-consistent calculation of the Hubbard parameters by a linear response (LR) approach, along with empirical sets selected from previous works are presented. Comparison of the aforementioned sets and their associated electronic behavior, with respect to the hybrid functional outcome, is addressed in Sec. III F. We conclude the paper with final remarks and giving an outlook for future work. Additional data and figures that complement the results and discussion presented in the main text have been left as Supplemental Material (SM) [24].

II. COMPUTATIONAL DETAILS

All calculations were carried out using the QUANTUM ESPRESSO package (QE) [25]. We use three types of functionals, namely, the standard Perdew-Burke-Ernzerhof (PBE) functional, a modified PBE functional with Hubbard corrections (also called DFT+U+V) according to implementations in Ref. [15] and the hybrid HSE06 (HSE) functional [26] with the ACE implementation [27]. Relaxed structures were obtained at PBE and DFT+U+V levels with a force tolerance of 10^{-2} eV/Å per atom and an energy tolerance of 10^{-8} Ry. A vacuum layer of 20 Å was used to simulate the layered character of the systems. The energy cutoff for the self-consistent calculations was set to 100 Ry for all cases with a tolerance of 10^{-8} Ry. Calculations included the possibility of magnetic final states without considering spin-orbit coupling, that is, a spin-polarized setting. The k-space Monkhorst-Pack grid was fixed to $15 \times 15 \times 1$ points for all calculations. In the case of the HSE functional, the Fock operator was calculated with a q-space grid of $5 \times 5 \times 1$ points.

For the LR calculations that allow the self-consistent computation of the Hubbard parameters, the HP code was used [28] as part of the QE suite. The code requires a self-consistent ground state calculation of QE as a starting point. We use the orthoatomic type of projectors for this calculation, which sets the basis for the occupations matrices (see Sec. III E) with Löwdin orthogonalized atomic orbitals. Well-converged results for the values of the parameters were obtained using a q-space grid with $5 \times 5 \times 1$ points and a tolerance of 10^{-7} eV for the response function χ, defined in Ref. [28].

III. RESULTS

A. Structural properties

As shown in Fig. 1(a), the nickel chalcogenides NiX_2 in the 1T phase can crystallize in monolayer form with a trigonal lattice structure. The transition metal is located at the corners of the unit cell forming a triangular sublattice while the chalcogen atoms form a buckled hexagonal sublattice. This structure is described by space group (SG) $P\bar{3}m1$ (No. 164) [29]. This symmorphic SG has 12 symmetries generated by spatial inversion I, a threefold rotation about an axis perpendicular to the monolayer plane, and a twofold rotation about an axis that is in the monolayer plane along the lattice vector $\boldsymbol{a_1} + \boldsymbol{a_2}$ [see Fig. 1(a) for the lattice vector representation]. The relaxed structure obtained from our calculations shows that a generic Ni atom is sixfold coordinated, and the NiX_6 subsystem forms a distorted octahedron. Thus, for instance, using $NiSe_2$, we obtained that the elongated Se-Ni-Se angle has a magnitude of 95.58°, departing from the ideal right angle. Additional data concerning lattice parameters and bond lengths arising from the first-principles calculations detailed below are presented

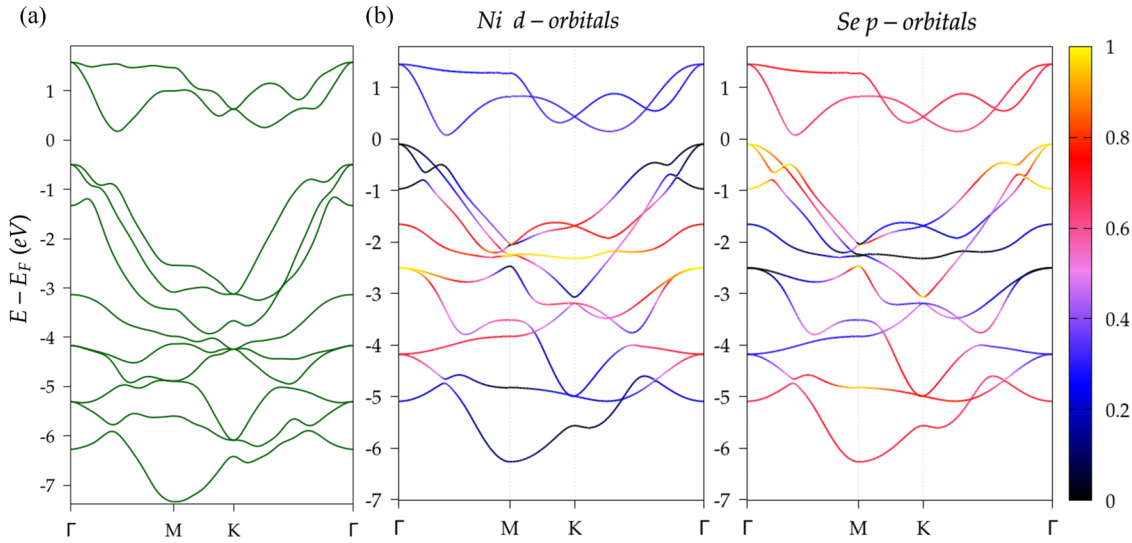

FIG. 2. (a) HSE electronic band structure for $NiSe_2$. (b) PBE electronic band structure with orbital projections for (left) Ni d-orbitals and (right) Se p orbitals. The color scale at the right is in states A^2/eV units.

in Table S.1 in the SM. The values reported in this paper agree well with previous studies [3,4,7].

One important consequence of the atomic landscape is that Ni atoms experience the well-known crystal field splitting associated to the interaction with chalcogen orbitals. This splitting can be directly deduced from the SG information by taking into account that the atom located at the unit cell corner (1a Wyckoff position to be more precise [30]), have a site symmetry isomorphic to point group (PG) $\bar{3}m1$. The dimensionality of the irreducible representations of this PG gives the maximal degeneracy that a set of orbitals can have. Using the tabulated information from the Bilbao Crystallographic Server [31], we can see that the greatest degeneracy that orbitals can have in this atomic environment is two. If we take into account the basis of atomic orbitals, we can see that, for example, d orbitals will split into three sets; one nondegenerate orbital and two sets of orbitals, each with a double degeneracy. The presence of these twofold degenerated orbitals will induce twofold degeneracies in momentum space. This real space momentum space relation will dictate the general form that the electronic structure will show in what follows.

B. Orbital order and first electronic structure description

Although correlated systems could be studied by more elaborate methods [9], we take here a mean-field approach as this can serve as a baseline for understanding the incidence of interactions in these TMD. The standard starting point of this approach is to perform an electronic structure at the level of the generalized gradient approximation (GGA) with the PBE functional. In the following, we present results for the $NiSe_2$ monolayer and refer the reader to the SM for analogous figures and data concerning the NiS_2 monolayer. First, we present the $NiSe_2$ electronic band structure in Fig. 2(b). The plot also contains information about the orbital projection along the high-symmetry path delimited by the high-symmetry points in the Brillouin zone, as represented in Fig. 1(b). The PBE projected bands show a clear tendency even at this level; upper valence bands have a clear p-orbital type coming from Se atoms. However, deep valence bands have a more mixed character, they are formed by the strong hybridization of Ni d orbitals and Se p orbitals, as expected by the features of the lattice structure. This orbital energy order is similar to the behavior observed in charge-transfer insulators [32]. Specifically, when the p orbitals are on top of the d orbitals in the valence bands, the material will present a small or even negative charge-transfer gap [32]. This charge transfer can be understood as the passing of electronic charge from the p shell at chalcogen atoms to the d shell belonging to the transition metal. This is formally represented as $d^n p^6 \rightarrow d^{n+1} p^5$ and in this type of system, this process will correspond to the low-energy excitations [33]. However, as is well-known, PBE results consistently underestimate localization effects and systematically tend to delocalize electrons [11], which results in a sometimes deficient prediction of the ground-state properties. For transition metal compounds, this is a well-documented issue and methods to improve the PBE results are needed to meet experiments [14]. Following this line, we will explore two levels of extension of the PBE results. In this section, we present the first one. In Fig. 2(a), the electronic band structure resulting from using a hybrid HSE functional is shown. This functional, by definition, includes a part of the exact exchange [26]. The hybrid band structure exhibits a gap of approximately 0.6 eV, which, as expected, is greater than the PBE band gap, which has a magnitude of ~0.1 eV. In the case of NiS_2, the hybrid gap is approximately 1.0 eV, while the PBE calculation yields a value of ~0.5 eV. Another difference stems from the dispersion of top valence bands and their interaction with deep valence bands. It can be observed that the HSE result yields a clear separation between the set of upper and lower valence bands and higher dispersion for the upper valence bands. These effects can be traced to including localization in the hybrid case. This can be observed if we study the real-space orbital character of $NiSe_2$ using the local density of states. In Fig. 3, we compare in more detail the

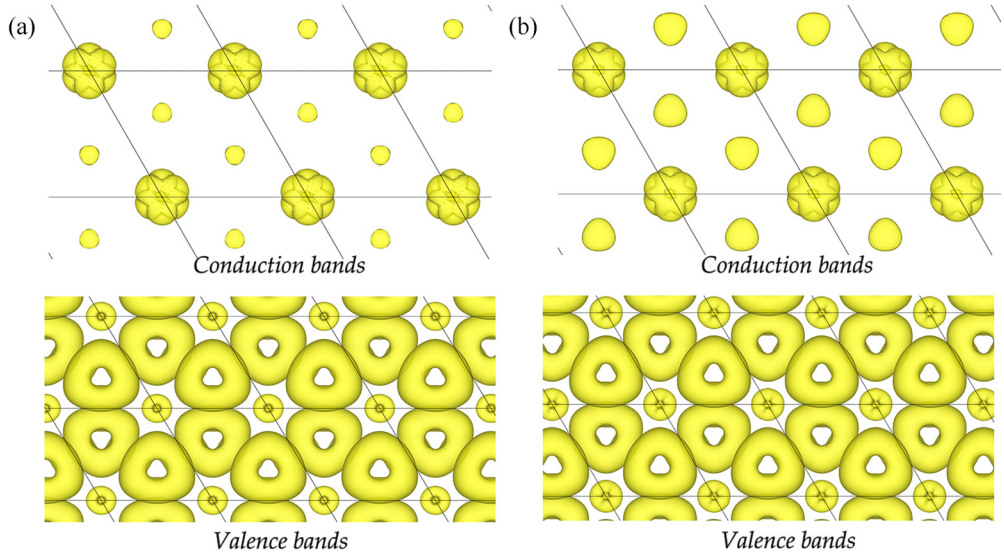

FIG. 3. (a) Integrated local density of states for (top panel) lowest conduction bands and (bottom panel) top of the valence bands with the HSE functional for $NiSe_2$. (b) Integrated local density of states for (top panel) lowest conduction bands and (bottom panel) top of the valence bands with the PBE functional for $NiSe_2$. In both cases, the valence band range is 0.4 eV from the top of the bands. The conduction band integration range goes from the Fermi level to 1.5 eV.

level of localization for the low energy range of the system obtained from the hybrid functional versus the PBE result, represented by the integrated local density of states (ILDOS). Although the results roughly coincide, a closer look shows that the *p*-orbital contribution to the conduction bands is more localized in the HSE case [Fig. 3(a), top] with respect to the PBE result [Fig. 3(b) top]. Also, for the upper valence bands, states situated at Ni atoms show a slightly more delocalized appearance in PBE [Fig. 3(b) lower panel] in comparison with the HSE case [Fig. 3(a), lower panel)]. The above discussion indicates that including electron correlations in monolayer NiX_2 materials should play a key role in describing properties derived from the electronic structure. In principle, we can stay with the hybrid functional as the final result. However, hybrid functionals suffer from technical complications related to the computational effort to calculate the exact exchange, and this fact hinders their utilization in broader applications. Also, these kinds of functionals also lack other contributions to correlation [9], and thus more sophisticated approaches should be used, such as *GW* calculations and dynamical mean-field methods. Despite this, the HSE result significantly improves the bare PBE calculation. Thus, in the following, we take the HSE ground state as a reference and compare it with another method that tries to improve on the PBE level by including Coulomb interactions at the mean-field level. It is worth mentioning that for the hybrid calculations, a spin-polarized calculation was carried out, allowing for a final magnetic ground state. Yet no magnetic state was observed in our calculations, even when changing the screening parameters.

C. DFT+*U*+*V* method

We have calculated the electronic structure of NiX_2 materials considering the inclusion of correlation through Hubbard parameters. We introduce the parameters by resorting to a simplified model to visualize this setting better. From the above calculations, we can identify the Ni *d* orbitals and the Se (S) *p* orbitals as the most important orbitals. Using a tight-binding representation with no correlation, the low-energy Hamiltonian takes the following form:

$$H_0 = \epsilon_d \sum_{\alpha} d_{\alpha}^{\dagger} d_{\alpha} + \epsilon_p \sum_{\beta} p_{\beta}^{\dagger} p_{\beta} + \sum_{\alpha\beta} t_{\alpha\beta} (d_{\alpha}^{\dagger} p_{\beta} + \text{H.c.}). \quad (1)$$

Here $d_{\alpha}^{\dagger}$ and $p_{\beta}^{\dagger}$ are the creation operators for an electron in *d* orbitals and *p* orbitals, respectively. The terms in the first line correspond to on-site energies, and the last term is the hopping parameter that serves to implement hybridization among Ni and Se orbitals. The inclusion of correlation is realized as an extended Hubbard model that is expressed as [32]

$$H_{UV} = H_0 + U_{Ni} \sum_{\alpha} n_{d_\alpha} n_{d_\alpha} + U_X \sum n_{p_\beta} n_{p_\beta} + V_{\text{Ni}X} \sum_{\langle \alpha\beta \rangle} n_{d_\alpha} n_{p_\beta} + V_{XX} \sum_{\langle\langle \beta\gamma \rangle\rangle} n_{p_\beta} n_{p_\gamma}, \quad (2)$$

where $X = \text{S, Se}$.

In this Hamiltonian, n_{d_α} and n_{p_β} denote the occupation operators for *d* and *p* orbitals, respectively. The second and third terms represent the so-called on-site Hubbard parameters that quantify the cost in energy of double occupancy for a *d* orbital (U_{Ni}) and a *p* orbital (U_X). The fourth term, with the coefficient $V_{\text{Ni}X}$, represents an extension of the theory to include the intersite interaction between occupations among the *d* and *p* orbitals. The last term is also an intersite interaction between the next-nearest neighbors of the Se-Se type in this class of materials. In practice, we include two of these (Se-Se) interactions; second and third neighbors. We stop at this level

and leave more distant correlations outside the subsequent calculations.

A DFT implementation of the interactions presented above, with a self-consistent and rotational invariant character, is employed for the calculation of the ground states. This level of theory is customarily denoted as DFT+U+V [15]. We do not enter into the details of the theory here as this has been extensively exposed in recent works [18,19]. We only mention that the formalism is based on the modification of the original DFT framework by the addition of a correction term $E_{U,V}$ giving a new energy functional $E = E_{\mathrm{DFT}} + E_{U,V}$. The key ingredients of the $E_{U,V}$ term are the so-called occupation matrices $n^{IJ\sigma}_{m,m'}$ which are defined by the projection of the Kohn-Sham eigenfunctions ψ^{σ}_{μ} (σ labels spin) on a set of localized orbitals ϕ^{I}_{m} (J labels the atomic site and m labels the orbital quantum number), such that [14]

$$n^{IJ\sigma}_{m,m'} = \sum_{\mu} f^{\sigma}_{\mu} \langle \psi^{\sigma}_{\mu} | \phi^{J}_{m'} \rangle \langle \phi^{I}_{m} | \psi^{\sigma}_{\mu} \rangle. \tag{3}$$

The coefficients accompanying these matrices are the Hubbard on-site and intersite parameters presented above. The $n^{IJ\sigma}_{m,m'}$ are obtained in a self-consistent way along the energy computation and comprise an appropriate model for interactions at the mean-field level, with the advantage of being part of a fast and flexible framework.

As has been made patent by the model presented, the Hubbard parameters will modify the localization character of the orbital manifolds of interest. However, until recently, the most used procedure was to set the parameters in a semiempirical way, resorting to experimental references or previous numerical benchmarks [34]. Presently, an alternative approach is to calculate these parameters in a self-consistent manner and various approaches have been made available [16,17,35].

To describe the reference hybrid calculations, we will put into practice a semiempirical procedure, which makes use of empirical parameters combined with the exploration of a LR calculation. In the first place, to achieve a general picture of the possible phases that the NiX_2 materials have at the DFT+U+V level, we construct phase diagrams based on several ground-state calculations. With this knowledge at hand, we explore different sets of parameters to assess the role of the various Hubbard corrections.

D. Magnetic phase diagrams

The possible magnetic phases of the systems at the mean-field level are identified by performing several DFT+U+V calculations within a range of values for U and V parameters, and the resulting phases are depicted in Figs. 1(a) and 1(b). The obtained states show the presence of only two cases: a nonmagnetic phase and a ferrimagnetic (FiM) phase with a completely compensated magnetization. The magnetic moment distribution for this FiM phase in real space is presented in the SM (Fig. S.9). The FiM phase is also metallic and suffers from an enlargement of the unit cell due to the increment of the interactions (see Table S.1 in the SM for a summary of the geometric parameters obtained for the magnetic phases). Observation of the trends in these calculations indicates that the FiM state is very robust, as it is the only ground state encountered for the range of values explored (without considering eventual lattice distortions that could change the SG symmetry). This FiM state appears even in the case where only U_{Ni} is nonzero. An antiferromagnetic coupling forms the FiM state among the Ni atoms and the surrounding chalcogen neighbors. Considering all these facts, we can expect that the final FiM state will be produced due to the difference in localization of the p electrons in comparison with d electrons; the more itinerant p electrons tend to metallize the system, while d electrons will tend to stay localized. In the overall, above a critical value U_C for on-site Ni interaction, which is of the order of ∼6.5 eV for both materials (when $\mathrm{U}_X = 0$), it will be favorable to produce a conducting channel with only one type of spin polarization, leaving the remaining channel insulating. The critical value U_C linearly decreases with an increasing magnitude of the on-site parameter U_X, thus forming a line of critical values U_C (U_X) in the phase diagram [see Fig. 1(a)].

On the other hand, we see that even when correlations are important, the system can have a nonmagnetic insulating state. These types of states could be similar to the ground state obtained with the hybrid calculation.

E. Linear response calculation and empirical parameters

In this section, we illustrate different calculations with various sets of parameters as stated before. We start by presenting the results of the LR method to see if it can give a state similar to our reference calculation. For this paper, we use the method formulated in Ref. [36]. The Hubbard parameters are computed within this framework using density functional perturbation theory. Section II presents the specific settings used for the calculations in this paper. We now outline the procedure that has been put forward for procuring a converged set of parameters. First, the calculation needs an initial guess for the Hubbard parameters. We have started from zero values and, with this set, run a first calculation. One of the subtle points is that our starting configuration concerns an insulating phase with no magnetic state. However, as is well-known, variations of the electron interaction strength could result in magnetic states and also in metal-insulator transitions [32]. Thereby, after the initial LR computation (first shot), we carried out a new ground-state computation with the obtained set of parameters. This ground state is now used as the input of a second shot for the LR calculation to see how parameters vary. After this shot, the procedure explained after the first shot is repeated until the magnitude of the parameters does not change above a desired tolerance. For our purposes, we set the threshold at 0.1 eV, where we noted that the electronic structure does not suffer appreciable changes for all the considered parameters. This iterative process yields the LR Hubbard parameters that are presented in Table I (labeled as set 1) for both NiS_2 and $NiSe_2$. The final phase obtained from LR is a magnetic metallic state; the already encountered FiM state. In particular, we find a nonzero absolute magnetization of ∼2.7 μ_B/cell for NiS_2 and ∼3.1 μ_B/cell for $NiSe_2$. The electronic band structures that are obtained for these parameters for both materials are presented in Figs. S.4– S.7 in the the SM. Therefore, in comparison with our reference calculation, the LR calculation does not give the correct ground state.

We now move on to consider other arrays of parameters that allow us to survey other areas of the phase space. To

TABLE I. Hubbard parameters for the different sets studied for NiS_2 and $NiSe_2$. The last column reports the values for the first-neighbor intersite interactions that give a band gap similar to the HSE hybrid calculation. All values are in eV units.

Parameter set	U_{Ni}	U_X	V_{NiX}	$V_{XX}^{(1)}$	$V_{XX}^{(2)}$	$V_{NiX}^{HSE-gap}$
NiS_2 set 1	6.79	3.84	0.68	0.51	0.47	1.80
NiS_2 set 2	5.00	2.00		0.51	0.47	1.80
NiS_2 set 3	5.00	0.00		0.00	0.00	1.70
NiS_2 set 4	2.00	0.00		0.00	0.00	1.70
$NiSe_2$ set 1	6.50	3.53	0.61	0.45	0.41	2.20
$NiSe_2$ set 2	4.50	1.50		0.45	0.41	2.20
$NiSe_2$ set 3	4.50	0.00		0.00	0.00	2.20
$NiSe_2$ set 4	1.5	0.00		0.00	0.00	2.00

motivate the selection of these sets, we consider the above LR calculation and also take into account previous results that employed Hubbard-corrected functionals. An important fact about parameters U and V is that their magnitudes are weakly dependent on the values taken by the rest of the parameters. That is to say, for example, if we adjust the U_{Ni} value in the calculation, the value obtained by only considering this parameter as nonzero does not change appreciably when adjusted in conjunction with the intersite parameters or with U_X. This allows us to consider the variation of each value independently.

If we now take into account the values of the on-site parameters used in previous works, we could see that the magnitudes explored for U_{Ni} range from 4 eV to 8 eV [37–40]. A well-known reference system is NiO, where in Ref. [34] values of 6.8 eV and 5.9 eV were obtained for U_{Ni} with and without considering the contribution of the O atom, respectively. These values indicate that the LR outcome is giving sensible results for U_{Ni}. However, if we want to make a comparison with a system closer to those of this work, one of the best candidates is the $NiS_{2-x}Se_x$ material with the pyrite structure [41,42]. This material is known to be a charge transfer insulator [41,43,44] and possesses a crystal field configuration for the Ni atom, similar to the NiX_2 materials analyzed here but in bulk form [39]. The most used values for U_{Ni} in these type of systems are 5 eV and 4.5 eV when considering S and Se, respectively [42]. These values are lower than the LR result. A possible explanation for this is that the magnitudes can be affected by the inclusion of the Hund exchange interaction J [32]. This interaction is not considered in the LR calculation in its present form.

For the case of onsite U_X interaction, we have found no reported values for the pyrite structure, but for NiO in Ref. [34] values for U_O in the range of 8 to 9 eV have been reported. Earlier results such as in Ref. [32], point that values of at least 3 eV should be used for the O atoms. This gives an idea that the chalcogen on-site parameter also have a sizable magnitude and therefore the values obtained for U_X in LR are in accordance with this behavior.

Inspired by the above-mentioned studies, we construct three additional sets of values. The values for each additional set are presented in Table I. In particular, the motivation for set 2 (for both materials) is to lower the on-site interactions to previously reported values for U_{Ni}, such that an insulating state with same intersite V_{XX} parameters as in the LR calculation is realized. In the case of set 3, we keep the same on-site interactions with respect to set 2 and take the intersite V_{XX} parameters to zero. Both sets, set 2 and set 3, try to simulate the effect that will have, for example, the inclusion of the Hund exchange on the onsite parameters. Finally, set 4 is a low correlation state that serves as a complementary comparison. As can also be noted from Table I, there are two entries for the nearest neighbor interaction V_{NiX}. The first entry is empty in most cases because, as described in the following section, V_{NiX} will be used as a variable that is related to the control of the charge transfer properties of NiX_2. The other entry is explained in the next section.

Thus, we will explore the implications of keeping most Hubbard parameter values fixed while varying the V_{NiX} parameter. A guideline that this is indeed plausible is that, observing the U_{Ni} versus V_{NiX} diagram in Fig. 1(d), even if we start in the FiM region and move horizontally in the graph to greater values of V_{NiX}, we invariably end in a nonmagnetic correlated state.

F. Band-gap energy and intersite Coulomb interaction

We now study how the electronic structure behaves under the variation of the intersite interaction V_{NiX} for the different sets in Table I. It is appropriate to stress that the V_{XX} interactions do not have a substantial impact on the properties of the systems. We have checked by further electronic structure calculations that varying V_{XX}, which are next-nearestneighbor parameters, the localization properties, band dispersion, and energy gap, are not significantly affected. This is the reason for keeping these values fixed for each set for the rest of the paper.

We first describe the computation with set 1 since it is the most complete case, as it encompasses both magnetic and nonmagnetic phases. The rationale is to increase V_{NiX} beyond values where a magnetic phase transition is produced, also implying a metal-insulator transition. Both transitions happen at almost the same V_{NiX} values. The trend observed in the process is that the absolute magnetization decreases when V_{NiX} grows. This happens up to a point where it abruptly goes to zero. The critical values found were $\sim$1.4 eV for NiS_2 and $\sim$1.8 eV for $NiSe_2$. This magnetic transition is also accompanied by a reduction of the lattice parameter of the unit cell in such a way that, after the transition, the system recovers the original lattice constant found in the noninteracting GGA calculation. As a result, the system will no longer have magnetic properties and will display an energy gap beyond this point. At this stage, the most notable aspect is that as the parameter increases, there is an increase in the energy gap of the system. In simpler terms, there is a direct relationship between the value of V_{NiX} and the gap size.

To see if this behavior is general for the nonmagnetic insulating phase, we take the other sets in Table I and perform band-structure calculations with varying V_{NiX}. From these calculations, we compute the dependency of the gap energy with respect to the intersite interaction and plot the results for NiS_2 and $NiSe_2$ in Fig. 5. It can be extracted from these results that the relation of intersite interaction with the size of the gap is robust and independent of the other Hubbard

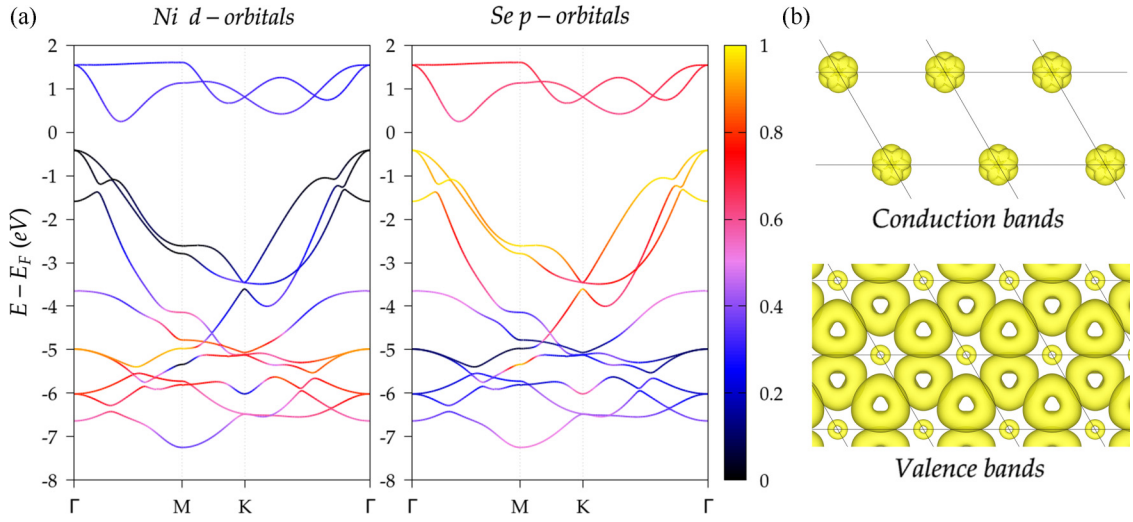

FIG. 4. (a) Orbital-projected electronic band structure at the DFT+U+V level of $NiSe_2$ with parameters from linear response with modified V_{NiX} parameter. The color scale at the right is in (states Å^2)/eV units. (b) Integrated local density of states for (top panel) lowest conduction bands and (bottom panel) top of the valence bands using the DFT+U+V functional with linear response parameters with modified V_{NiX}.

parameters. This provides solid evidence that the main ingredient for describing the charge transfer effects in these systems at the DFT+U+V level is the intersite interaction. As an additional supporting calculation, we have tried to test the effect of using only the U interaction on the energy gap. We found that obtaining the same effects using only DFT+U is not feasible. In the SM, we includ a calculation at this level for the NiS_2 case in Fig. S.8.

We can now compare the above-studied cases with the hybrid functional results. We must select a value for V_{NiX} for this. The criterion is to match the energy gap magnitude obtained from the HSE calculation. We present the values that meet this requirement in the last column of Table I. It can be seen that for all sets studied, the value of the intersite interaction $V_{NiX}^{HSE-gap}$ is similar, which suggests that the relationship is sufficiently reliable.

As a representative example of the role of all parameters, in Fig. 4(a) we present a band-structure calculation for set 1 (using $V_{NiX}^{HSE-gap}$), together with orbital localization information in the form of an ILDOS in Fig. 4(b). It can be recognized right away that the inclusion of correlation improves not only the band-gap magnitudes but also gives a more localized character to the states for both Ni d orbitals and Se p orbitals, which is mainly the effect of including the on-site U parameters (a similar calculation for NiS_2 is available in Figs. S.1 and S.2 in the SM). Also, the dispersion of the top valence bands becomes very similar to the hybrid bands in Fig. 2(a). This can be verified by looking at the energy range that the two top valence bands span in Fig. 4(a). A rough estimate gives that these bands cover 2.8 eV, similar to the 2.5 eV that the same bands cover in the hybrid bands. This is a significant upgrade over the PBE result, which only spans 1.9 eV. Similar outcomes are obtained for NiS_2 as presented in Fig. S.3 in the SM.

The band-gap dependence on V_{NiX} as displayed in Fig. 5 can be linked to the charge transfer properties of the materials. As discussed previously, without Hubbard corrections, the system already shows an inverted valence band ordering similar to the case of transition metal oxides [32]. At this PBE level, if final orbital manifold occupations are computed, it is obtained that for Ni atoms there exists a considerable outer shell occupation of ∼9.2. Formally, Ni must be in a state with d^6. Conversely, the p shell of each Se (S) atom finishes with an occupation of 4.4. Formally, the initial state of this manifold is p^6. Thus, we have evidence that a charge transfer has occurred, where the p-shell occupation of each chalcogen atom has changed by approximately 1.5. This implies a p-hole formation, a well-known phenomenon in these charge transfer systems [33]. The inclusion of correlations alters occupations slightly. However, the tendency gives us clues about the behavior of the electronic structure. Thus, if we turn on correlations with nonzero Hubbard parameters, the occupation of the Ni d shell decreases, and increases for the Se (S) p shell. This is understandable because the rise in electronic localization hinders charge transfer. However, the system remains in the charge transfer regime as p orbitals continue to be higher in energy with respect to d orbitals.

If we start in a FiM phase, and V_{NiX} moves to higher values for the range where the system is still in the FiM state; the charge transfer process shows an opposite pattern of evolution for different atoms and spins. That is, for the chalcogen atoms, the majority spins get their occupations diminished while the minority spins achieve greater occupations. In the case of the Ni atoms, the behavior gets reversed. This mechanism conflates so the spin unbalance at each atom is utterly canceled.

If we start from a nonmagnetic phase or achieve it from a phase transition from the FiM state (both cases are equivalent), the augmentation of V_{NiX} reduces the charge transfer. This reduction is coupled with a new increase in localization, which competes with the orbital mixing between Ni and Se (S) atoms, The former is traduced in energy-level repulsion. This implies that bonding d orbitals will get deeper in energy, separating from the bands with a predominantly p-type character. Thus, the corresponding antibonding orbitals associated with

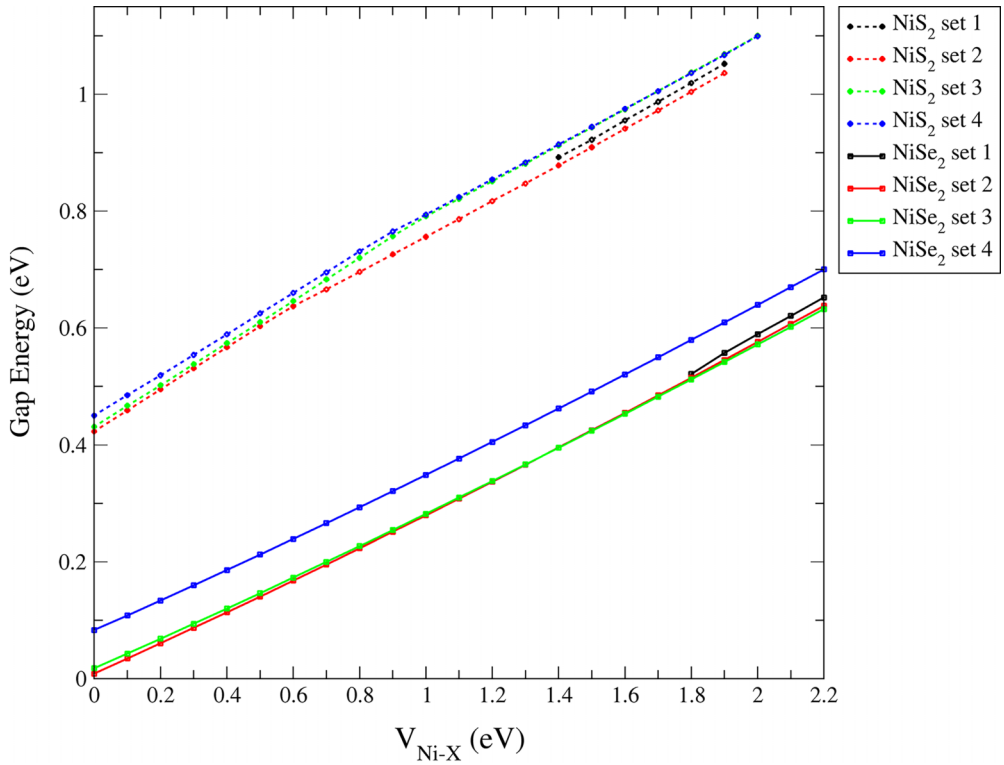

FIG. 5. Band-gap energy dependence on the nearest-neighbor interaction V_{NiX} for the sets in Table I for NiS_2 and $NiSe_2$.

the lower conduction bands will increase their energy. Overall, the band gap grows, controlled by the value of the intersite interaction. In other words, the increase of V_{NiX} will make the generation of charge-transfer excitations energetically more costly, which traduces in a greater band gap.

IV. DISCUSSION AND CONCLUDING REMARKS

To put in perspective the findings obtained, we can make a few additional remarks. First, although the PBE level already shows distinctive indicators of the charge transfer state, such as the inverted band ordering, correlations must be included in this type of system since it is a crucial competing mechanism for covalency and orbital hybridization. As shown above, it is the correlation that defines the magnitude of the energy band gap, the valence band dispersion, and orbital localization, which are important, for example, to study optical responses. Also, sufficiently high on-site correlations must be present in the system to realize a charge transfer insulating state, as outlined in the Zaanen-Sawatzky-Allen scheme [32,45].

Regarding the LR calculation, although this phase does not seem to be the one that experimentally materializes [4], we found that the calculation is useful to get an idea of the order of magnitude of the parameters that the systems could have. Also, considering the technical part, we have tried to amend the outcome by starting from different insulating and metallic states and, ultimately, the calculation consistently tends to the featured magnetic phase. This could be linked to several aspects. First, there is an already recognized issue related to calculations on systems with a nearly full shell [28,36]. Complementarily, the method does not include the Hund exchange interaction, which, as we mentioned earlier, can be important in these systems. Another issue to consider is the adequate inclusion of Coulomb screening in the parameter calculation as indicated, for example in Ref. [46]. Notwithstanding, the LR calculation is only a guide that does not have incidence in the main results of this paper. Then, the sets of parameters presented here are valuable prospects for performing future physical response computations involving electronic correlation.

Viewing the entire array of results, if the insulating phase is corroborated in subsequent studies, the charge transfer phase will be an interesting system to analyze further. This is because, as has been identified in other works, the *p*-hole formation, also known as self-doping, could lead to other effects when the system is perturbed [32,33,47,48]. The interplay between the 2D character of the materials and this *p*-orbital dominance could also lead to interesting phenomena.

In summary, we have put forward a detailed analysis of the electronic structure of monolayer TMDs NiS_2 and $NiSe_2$, using a variety of first-principles methods. This allows us to ponder the role that electronic interaction plays at the mean-field level. A hybrid HSE functional was used as the first reference in that the inclusion of correlations is built-in in its formulation. Comparison with modern Hubbard-corrected PBE functionals allowed further understanding of the importance of localization and the relation to the charge transfer effect. We demonstrate that nearest-neighbor intersite parameter V_{NiX} is directly linked to the the energy band gap of the ground state, as this interaction competes with the Ni-*X* hybridization and controls the energy of the charge-transfer

excitations. In the future, further analysis of this problem will focus on enhancing the inclusion of correlation through more advanced calculations, such as *GW* calculations. Investigating how the DFT+U+V method measures up against other state-of-the-art approaches would be quite intriguing. It would also be interesting to explore how to improve the self-consistent computation of Hubbard parameters for these systems such that results agree with other first-principles methods. Ultimately, our goal is to highlight the importance of including more interaction parameters in studies like this. Doing so could offer insights into the behavior of correlated systems.

ACKNOWLEDGMENTS

This paper has been supported by the Postdoctoral Grant from Universidad Técnica Federico Santa María, and Chilean Fondo Nacional de Desarrollo Científico y Tecnológico Grant No. 1220700.

[1] S. Manzeli, D. Ovchinnikov, D. Pasquier, O. V. Yazyev, and A. Kis, 2D transition metal dichalcogenides, Nat. Rev. Mater. **2**, 17033 (2017).

[2] J. Zhou, L. Shen, M. D. Costa, K. A. Persson, S. P. Ong, P. Huck, Y. Lu, X. Ma, Y. Chen, H. Tang, and Y. P. Feng, 2DMatPedi, an open computational database of two-dimensional materials from top-down and bottom-up approaches, Sci. Data **6**, 86 (2019).

[3] M. N. Gjerding, A. Taghizadeh, A. Rasmussen, S. Ali, F. Bertoldo, T. Deilmann, N. R. Knøsgaard, M. Kruse, A. H. Larsen, S. Manti, T. G. Pedersen, U. Petralanda, T. Skovhus, M. K. Svendsen, J. J. Mortensen, T. Olsen, and K. S. Thygesen, Recent progress of the computational 2D materials database (C2DB), 2D Mater. **8**, 044002 (2021).

[4] Y. Shao, S. Song, X. Wu, J. Qi, H. Lu, C. Liu, S. Zhu, Z. Liu, J. Wang, D. Shi, S. Du, Y. Wang, and H.-J. Gao, Epitaxial fabrication of two-dimensional $NiSe_2$ on Ni(111) substrate, Appl. Phys. Lett. **111**, 113107 (2017).

[5] H. Khalatbari, S. I. Vishkayi, M. Oskouian, and H. R. Soleimani, Band structure engineering of Ni2 monolayer by transition metal doping, Sci. Rep. **11**, 5779 (2021).

[6] Anisha, R. Kumar, S. Srivastava, and K. Tankeshwar, Optimising 1T-NiS_2 monolayer thermoelectric performance via valley engineering, Mater. Today Commun. **34**, 105169 (2023).

[7] R. Ku, L. Yan, K. Xue, J. Zhang, K. Pang, M. Sha, B.-T. Wang, Y. Jiang, L. Zhou, and W. Li, NiX_2 (X = S, Se, and Te) monolayers: Promising anodes in Li/Na-Ion batteries and superconductors, J. Phys. Chem. C **126**, 6925 (2022).

[8] I. N. Levine, D. H. Busch, and H. Shull, *Quantum Chemistry* (Pearson Prentice Hall, Upper Saddle River, NJ, 2009), Vol. 6.

[9] R. M. Martin, L. Reining, and D. M. Ceperley, *Interacting Electrons: Theory and Computational Approaches* (Cambridge University Press, Cambridge, 2016).

[10] A. Altland and B. D. Simons, *Condensed Matter Field Theory*, 2nd ed. (Cambridge University Press, New York, 2010).

[11] R. M. Martin, *Electronic Structure: Basic Theory and Practical Methods* (Cambridge University Press, Cambridge, 2004).

[12] R. J. Bartlett and M. Musiał, Coupled-cluster theory in quantum chemistry, Rev. Mod. Phys. **79**, 291 (2007).

[13] V. I. Anisimov, I. V. Solovyev, M. A. Korotin, M. T. Czyżyk, and G. A. Sawatzky, Density-functional theory and NiO photoemission spectra, Phys. Rev. B **48**, 16929 (1993).

[14] M. Cococcioni and S. de Gironcoli, Linear response approach to the calculation of the effective interaction parameters in the LDA + U method, Phys. Rev. B **71**, 035105 (2005).

[15] V. L. Campo and M. Cococcioni, Extended DFT +U+V method with on-site and inter-site electronic interactions, J. Phys.: Condens. Matter **22**, 055602 (2010).

[16] J. Huang, S.-H. Lee, Y.-W. Son, A. Supka, and S. Liu, First-principles study of two-dimensional ferroelectrics using self-consistent Hubbard parameters, Phys. Rev. B **102**, 165157 (2020).

[17] N. Tancogne-Dejean and A. Rubio, Parameter-free hybridlike functional based on an extended Hubbard model: DFT+U+V, Phys. Rev. B **102**, 155117 (2020).

[18] M. Cococcioni and N. Marzari, Energetics and cathode voltages of LiMPO4 olivines (M = Fe, Mn) from extended Hubbard functionals, Phys. Rev. Mater. **3**, 033801 (2019).

[19] C. Ricca, I. Timrov, M. Cococcioni, N. Marzari, and U. Aschauer, Self-consistent DFT+U+V study of oxygen vacancies in $SrTiO_3$, Phys. Rev. Res. **2**, 023313 (2020).

[20] R. Mahajan, I. Timrov, N. Marzari, and A. Kashyap, Importance of intersite Hubbard interactions in β-MnO_2: A first-principles DFT+U+V study, Phys. Rev. Mater. **5**, 104402 (2021).

[21] J. Yang, T. Zhu, and S. Liu, Onsite and intersite electronic correlations in the Hubbard model for halide perovskites, Phys. Rev. B **106**, 195159 (2022).

[22] I. Timrov, F. Aquilante, M. Cococcioni, and N. Marzari, Accurate electronic properties and intercalation voltages of olivine-type Li-Ion cathode materials from extended Hubbard functionals, PRX Energy **1**, 033003 (2022).

[23] B. G. Jang, M. Kim, S.-H. Lee, W. Yang, S.-H. Jhi, and Y.-W. Son, Intersite coulomb interactions in charge-ordered systems, Phys. Rev. Lett. **130**, 136401 (2023).

[24] See Supplemental Material at http://link.aps.org/supplemental/10.1103/PhysRevB.108.235138 for additional results from first-principles calculations, concerning structural information, and electronic properties.

[25] P. Giannozzi, O. Andreussi, T. Brumme, O. Bunau, M. B. Nardelli, M. Calandra, R. Car, C. Cavazzoni, D. Ceresoli, M. Cococcioni, N. Colonna, I. Carnimeo, A. D. Corso, S. de Gironcoli, P. Delugas, R. A. DiStasio Jr, A. Ferretti, A. Floris, G. Fratesi, G. Fugallo *et al.*, Advanced capabilities for materials modelling with Quantum Espresso, J. Phys.: Condens. Matter **29**, 465901 (2017).

[26] J. Heyd, G. E. Scuseria, and M. Ernzerhof, Hybrid functionals based on a screened Coulomb potential, J. Chem. Phys. **118**, 8207 (2003).

[27] L. Lin, Adaptively compressed exchange operator, J. Chem. Theory Comput. **12**, 2242 (2016).

[28] I. Timrov, N. Marzari, and M. Cococcioni, HP—A code for the calculation of hubbard parameters using density-functional perturbation theory, Comput. Phys. Commun. **279**, 108455 (2022).

[29] H. T. Stokes and D. M. Hatch, *FINDSYM*: Program for identifying the space-group symmetry of a crystal, J. Appl. Crystallogr. **38**, 237 (2005).

[30] C. Bradley and A. Cracknell, *The Mathematical Theory of Symmetry in Solids: Representation Theory for Point Groups and Space Groups* (Oxford University Press, New York, 2010).

[31] L. Elcoro, B. Bradlyn, Z. Wang, M. G. Vergniory, J. Cano, C. Felser, B. A. Bernevig, D. Orobengoa, G. de la Flor, and M. I. Aroyo, Double crystallographic groups and their representations on the Bilbao Crystallographic Server, J. Appl. Crystallogr. **50**, 1457 (2017).

[32] D. I. Khomskii, *Transition Metal Compounds* (Cambridge University Press, Cambridge, 2014).

[33] F. Wrobel, H. Park, C. Sohn, H.-W. Hsiao, J.-M. Zuo, H. Shin, H. N. Lee, P. Ganesh, A. Benali, P. R. C. Kent, O. Heinonen, and A. Bhattacharya, Doped NiO: The Mottness of a charge transfer insulator, Phys. Rev. B **101**, 195128 (2020).

[34] M. Yu, S. Yang, C. Wu, and N. Marom, Machine learning the Hubbard U parameter in DFT+U using Bayesian optimization, npj Comput. Mater. **6**, 180 (2020).

[35] H. J. Kulik, M. Cococcioni, D. A. Scherlis, and N. Marzari, Density functional theory in transition-metal chemistry: A self-consistent Hubbard U approach, Phys. Rev. Lett. **97**, 103001 (2006).

[36] I. Timrov, N. Marzari, and M. Cococcioni, Hubbard parameters from density-functional perturbation theory, Phys. Rev. B **98**, 085127 (2018).

[37] A. E. Bocquet, T. Mizokawa, T. Saitoh, H. Namatame, and A. Fujimori, Electronic structure of 3d-transition-metal compounds by analysis of the 2p core-level photoemission spectra, Phys. Rev. B **46**, 3771 (1992).

[38] L. Wang, T. Maxisch, and G. Ceder, Oxidation energies of transition metal oxides within the GGA + U framework, Phys. Rev. B **73**, 195107 (2006).

[39] J. Kuneš, L. Baldassarre, B. Schächner, K. Rabia, C. A. Kuntscher, D. M. Korotin, V. I. Anisimov, J. A. McLeod, E. Z. Kurmaev, and A. Moewes, Metal-insulator transition in $NiS_{2-x}Se_x$, Phys. Rev. B **81**, 035122 (2010).

[40] P. Reiss, S. Friedemann, and F. M. Grosche, Ab initio electronic structure of metallized NiS_2 in the noncollinear magnetic phase, Phys. Rev. B **106**, 205131 (2022).

[41] A. Y. Matsuura, Z. X. Shen, D. S. Dessau, C. H. Park, T. Thio, J. W. Bennett, and O. Jepsen, Electronic structure and the metal-insulator transition in $NiS_{2-x}Se_x$, Phys. Rev. B **53**, R7584 (1996).

[42] L. Sangaletti, F. Parmigiani, T. Thio, and J. W. Bennett, Electronic-correlation effects in the x-ray-photoemission spectra of NiS_2, Phys. Rev. B **55**, 9514 (1997).

[43] A. Y. Matsuura, H. Watanabe, C. Kim, S. Doniach, Z.-X. Shen, T. Thio, and J. W. Bennett, Metal-insulator transition in $NiS_{2-x}Se_x$ and the local impurity self-consistent approximation model, Phys. Rev. B **58**, 3690 (1998).

[44] S. R. Krishnakumar and D. D. Sarma, X-ray photoemission study of $NiS_{2-x}Se_x$ (x=0.0–1.2), Phys. Rev. B **68**, 155110 (2003).

[45] J. Zaanen, G. A. Sawatzky, and J. W. Allen, Band gaps and electronic structure of transition-metal compounds, Phys. Rev. Lett. **55**, 418 (1985).

[46] B.-L. Liu, Y.-C. Wang, Y. Liu, Y.-J. Xu, X. Chen, H.-Z. Song, Y. Bi, H.-F. Liu, and H.-F. Song, Comparative study of first-principles approaches for effective Coulomb interaction strength Ueff between localized f-electrons: Lanthanide metals as an example, J. Chem. Phys. **158**, 084108 (2023).

[47] M. V. Mostovoy and D. I. Khomskii, Orbital ordering in charge transfer insulators, Phys. Rev. Lett. **92**, 167201 (2004).

[48] J. Kuneš, V. I. Anisimov, S. L. Skornyakov, A. V. Lukoyanov, and D. Vollhardt, NiO: Correlated band structure of a charge-transfer insulator, Phys. Rev. Lett. **99**, 156404 (2007).